Assessing heat vulnerability of New Orleans using multitemporal remote sensing and demographic data

Zijun Li

Abstract:

Coastal areas are more sensitive to climate change and are more vulnerable to increase in temperatures. For the last decades, residents of New Orleans have been experiencing hotter summer temperatures conditions and extreme weather conditions. Meanwhile, with economic development and the impact of human activities, the land cover of the region has experienced substantial changes. Since Hurricane Katrina in 2005, Parks and Parkway has undertaken a re-greening effort to replace the many thousands of trees lost. A specific benefit of tree cover is its ability to reduce the heat storage capacity of urban surfaces that creates urban heat islands. This study (1) creates an up-to-date, high spatial resolution land cover map and examine how the components of Land cover, particularly trees vary across post-Katrina New Orleans; (2) quantifies the magnitude and seasonality of LST change between 2006 to 2020 within the same areas of Land cover maps; and (3) contextualizes Land cover and LST patterns with census-based demographic data and to draw inferences about the heat vulnerability implications.

Keywords: Land cover, tree cover, Land surface temperature, health insurance

Table of Contents

1. Introduction:

Urban land use and land cover (LULC) mapping has been one of the major applications in remote sensing of the urban environment. Land cover refers to the biophysical materials at the surface of the earth (i.e., grass, trees, soils, concrete, water) (Liu, 2020). Tree cover is one of the most important components of Land cover in urban areas, and it is widely believed to provide myriad health services, which are crucial for urban sustainability (Wu 2010, 2013). These services include regulation of climate and water cycles (Bolund and Hunhammar 1999; Zhou et al. 2011), noise reduction (Pathak et al. 2011), air pollution mitigation (Yang et al. 2005; Nowak et al. 2006), reduced energy use (Ng et al. 2012), increased property values (Tajima 2003), and improved aesthetics (Home et al. 2010). A specific benefit of tree cover is its ability to reduce the heat storage capacity of urban surfaces that creates so-called urban heat islands (UHI) (Oke, 1982, Taha, 1997, Rizwan et al., 2008). Local difference in temperatures creates a negative impact on people and environment because negatively impacts air quality, increases energy consumption, loses biological control, and affects people's health (Kikegawa et al., 2003, Grimmond, 2007, Meineke et al., 2014, Plocoste et al., 2014, Tran, Duy X., et al, 2017). Climate risk prone areas like New Orleans experience multiple stressors in the absence of trees for reducing vulnerability to flooding caused by hurricanes and sea-level rise, and extreme heat from climate change. Understanding the long-term trajectories of tree provision is vital for assessing vulnerabilities and illuminating best practices for its development.

New Orleans has long been the subject of much study related to environmental hazards and the risk and equitable provision of environmental goods due to its unique vulnerabilities as a hurricane prone area, and historical inequities. Much study has focused on environmental provisions pre and post hurricane using surveys of trees, shrubs, and herbaceous lawns and the

composition and structure of plant communities across New Orleans (Lewis, Joshua A., et al, 2017). Such study has found a linkage between vegetation loss following catastrophic flooding (Potter, 2005). Vegetation loss and lack of regrowth is often experienced at a greater rate in Black and Brown neighborhoods as these areas are low lying and flood prone (Lewis, Joshua A., et al, 2017). For example, both Joshua and Potter found lagging vegetation disparities for these groups following Hurricane Katrina. Remote sensing has likewise been used to capture Land surface temperature(Kilic et al., 2016) and assess flood vulnerabilities (Randall et al., 2018) utilizing earth observations from 2013 to 2017 to assist groundwork New Orleans in reducing flood vulnerability.

Despite there being many articles analyzing vegetation effects on physical health in New Orleans, very little analysis has leveraged remote sensing for comprehensive change detection of tree cover over time. Remote sensing can be a valuable tool examining trajectories of tree cover change, and analyzing vulnerability due to lack of trees for specific neighborhoods (Gibbes, Cerian, et al). Despite its broad applicability in many applications, challenges can exist for multitemporal change detection when using remote sensing. Temporal coverage (return rates), obsolete and sensors that are no longer in service and data availability (spatial coverage) can all contribute to the issues in reconstructing land change processes with sufficient fidelity for accurate comparisons over time periods of interest. The adoption of multi-sensor data could potentially make up for missing temporal returns. Challenges persist in comparison that might be of different resolution, varying spectral quality for classifications and differing requirements for processing. However, testing the efficacy of using different sensors for change detection can add important insight into how these multitemporal dataset can be constructed in practice (Civco, Daniel L., et al, 2002).

In addition, remote sensing can help detect the secondary environmental risk to health by measuring land surface temperature (LST). LST approximates how temperatures can be experienced for urban residents as a general indicator of heat hazards(Wang, Jiong, et al. , 2019). Satellite-derived LST is widely used in a variety of applications, including land cover and land-cover change analysis (Lambin and Ehrlich, 1997), estimation and parameterization of surface fluxes (Lu et al., 2013), climate change studies (Hansen et al., 2010), vegetation monitoring (Kogan, 2001), urban climate studies (Voogt and Oke, 2003), and drought monitoring and surface soil moisture estimation (Wan et al., 2004a; Leng et al., 2014; Zhao et al., 2017a). Traditionally air temperature has been measured from ground stations, and this is a more accurate indicator of how individuals experience heat(Nichol, Janet E., et al, 2009). The challenge with this method is that ground stations are sparse and may not be located in communities where extreme heat is experienced. LST derived from remote sensing data allows for complete measure across neighborhoods and is a unique source of information for defining urban heat islands (Weng et al., 2004, Weng, 2009, Imhoff et al., 2010). It is retrieved based on thermal infrared sensors, using different surface emissivity sources. Despite the salience of pre-hazard to post-hazard change in LST due hurricanes, that often includes dramatic changes in land cover composition and resulting LST, long-term there have been few studies that use the unique capabilities of remote-sensing following disasters in New Orleans. Besides, there has been minimal research relating LST, land cover and vulnerability in the region. Examining the change/rise in urban heat islands in New Orleans as a result of natural disasters and development will help us understand potential changes in quality of life.

While LST allows for assessing heat exposure, it does not indicate health risks, which are associated with baseline health scores, behavioral exposure and access to health care. Critically in the United States, health coverage through health insurances is a strong indicator of health risk. According to the

Louisiana Health Insurance Survey in 2017 and regions defined by the Department of Health and Hospitals administrative regions, New Orleans ranks 6th with estimated uninsured children (under 19) and 4th with estimated uninsured adults by 9 regions (New Orleans, Baton Rouge, Houma-Thibodaux, Acadiana, Southwest, Central, Northwest, Northeast, Northshore). Additionally, the survey shows the percentage of children responding to insurance meets their needs is 71 percent and that of adults is 53 percent. Examining the health insurance coverage around neighborhoods can provide references for regions that are vulnerable in terms of disparities in heat exposure and re-greening effects.

The goals of this study are to: (1) create an up-to-date, high spatial resolution land cover map and examine how the components of Land cover, particularly trees vary across post-Katrina New Orleans; (2) quantify the magnitude and seasonality of LST change between 2006 to 2020 within the same areas of Land cover maps; and (3) contextualizes Land cover and LST patterns with census-based demographic data and to draw inferences about the heat vulnerability implications.

2. Methods

2.1 Study Area

New Orleans, Louisiana (NOLA) lies on the Mississippi River, near the Gulf of Mexico with a total area of 1084 km2 inhabited by almost 1,262,888 people, with an average density of 1165/km2. The latitude of New Orleans, LA, USA is 29.951065, and the longitude is -90.071533. New Orleans is subtropical with an annual high temperature of 25 °C, an annual low of 16.8 °C, and average annual precipitation of 162.3 cm. Average highest precipitation occurs in July (17.9 cm). The study area (Fig. 1) includes

communities in Lake View, Gentily, Esplanade Ridge, Treme, French
Quarter, Marigny, Mid-City, Downtown, Arts/Warehouse District, Uptown.

Fig 1. New Orleans case study area and major neighborhoods

2.2 Data Sources and Methods

To analyse the dynamic of vegetation and temperature for NOLA after Hurricane Katrina, we collected and processed several datasets derived from remote sensing (Table. 1). Our land classification is based on, High Resolution Orthoimages (2006 - 2012) and Sentinel-2 MultiSpectral Instrument, Level-1C(2012 -2018) imagery. For LST we used Landsat7 and Landsat8 data sets. Image processing was conducted in the Google Earth Engine application. Additional vulnerability mapping was done at the scale of the U.S. Census Tracts to be able to summarize key vulnerabilities at the neighborhood level using ArcGIS. The flow of methods is described in Fig. 2.

Dataset	Date	Resolution	Sources
Global Forest Change	2000 - 2019	30 meter	Global Land Analysis and Discovery
High Resolution Orthoimagery	2004, 2006, 2008, 2012	1 meter	USGS
Sentinel-2 MSI: MultiSpectral Instrument, Level-1C	2018, 2020	10 meter	European Space Agency
Landsat 7	2000-2012	30 meter	USGS
Landsat 8	2012-2020	30 meter	USGS
New Orleans Census Tracts	2021	Neighborhood statistical level	U.S. Census Bureau
TIGER/Line with selected Demographic and Economic data	2017	Community statistical level	U.S. Census Bureau

Table 1. Data information

Landsat 7
(ETM+),
Landsat 8
(OLI & TIRS)

High-resolution
orthoimages,
Sentinel-2 MSI

Calculate Land
Surface
Temperature

Pre-processing

U.S. Census
Bureau

Principal
component
analysis

Random forest
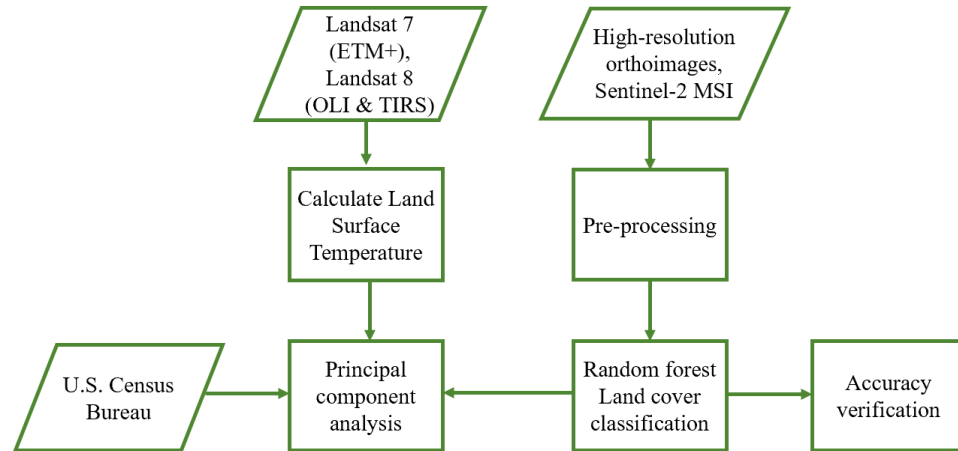Land cover
classification

Accuracy
verification

Fig. 2 Overview of the methodology

2.2.1 High resolution land cover classification and accuracy verification

2.2.1.1 Pre-processing

Terrain and geometrical correction were performed on the High Resolution Orthoimagery and Sentinel-2 MSI for spatial co-registration. We used a first-order polynomial method for geometric referencing (Fig. 2B; ESRI, 2014). Referencing results showed only minor offset between the two images with the x-direction deviation of 240 m and the y-direction deviation of 150 m, which may be related to the different ground control points (GCPs) used by the satellite image product processing teams. The total RMS error of correction was 0, which satisfied the accuracy requirement. Data was clipped to the New Orleans boundary and projected into Universal Transverse Mercator (UTM), Zone 15 with the North American Datum of 1983 (NAD83). The Orthoimages were aggregated up to a 10-meter scale to match the resolution of Sentinel-2 data.

2.2.1.2 Random forest classification and accuracy verification

We used Random Forest (RF) Machine Learning algorithms to classify land cover for the study area. RF has been widely used for classification (Breiman,

Leo, 2001, Zafari, 2019)Briefly, RF is an ensemble classifier that performs well in land classification. Moreover, RF is known for being fast, stable against overfitting and requiring small sample size with high dimensional input compared to many classifiers (Belgiu, Mariana, and Lucian Drăguț, 2016, Chan, Jonathan Cheung-Wai, et al, 2012). Classification is based on a "majority of vote" from assemblages of built trees (i.e. forests) that predict best class-assignment for any given pixel (Berhane, Tedros M., et al, 2018). Each tree is grown by recursively partitioning the data into nodes until each of them contains very similar samples, or until meeting one stopping condition. RF uses the Gini Index to find the best features (e.g reflectance) and plot points to separate the training samples (e.g. Manual examples of land cover classes) into homogeneous groups (classes). A key characteristic of RF is that only a random subset of all the available features is evaluated when looking for the best split point. The number of features in the subset is controlled by the user and is typically called *mtry*. Hence, for large trees which is what RFs use, it is at least conceivable that all features might be used at some point when searching for split points whilst growing the tree. The final classification results are obtained by considering the majority votes calculated from all trees. We classified 5 land cover classes (i.e., water, soil and barren, tree and forest, grass and herbaceous, impervious surfaces) based on the Meter-Scale Urban Land Cover (MULC) classification developed for the United States Environmental Protection Agency (US EPA) EnviroAtlas. The MULC classes are intended to represent common urban landscape composition and features that can be reliably identified in 1×1 m pixels, visible near-infrared digital aerial photography, by human aerial photo interpreters, and by computer image classification algorithms (Pilant, Andrew, et al, 2020). Training data were collected for the land cover classes using randomly chosen sites. Precision testing was conducted using the Kappa index and the overall accuracy for the classification (Congalton, Russell G, 1991, Keshtkar, Hamidreza, Winfried Voigt, and Esmaeil Alizadeh, 2017). Classification was

conducted using software Google Earth Engine and ENVI and pre and post processing analysis in Arc Pro.

In this study, 221 polygons for High resolution orthoimagery and 192 polygons for Sentinel-2 MSI are randomly selected to assess classification accuracy. The validation data are randomly and manually chosen based on Google Maps. Table (Classification accuracy verification values) contains the evaluation results of the five periods of images. Producer's accuracy and user's accuracy are obtained by a confusion matrix.

2.2.2 Land Surface temperature

LST is sensitive to vegetation and soil moisture, with land use/land cover changes drastically impacting it in urban contexts (ref). To capture corresponding LST changes from vegetation change, we calculated LST for all years using remotely sensed data retrieved from Landsat 7 and 8 dataset according to the procedure as described by Chander et al. (2009). It is calculated based on radiance values from which temperature can be inferred (i.e., black body temperature) followed by a correction for spectral emissivity according to the nature of the landscape (Weng et al. 2004). For instance, Impervious surface results in hotter temperatures than vegetation, water and surrounding areas. LST maps with band 6 (Landsat-7), band 10 (Landsat 8) and top of atmosphere brightness temperature values have been expressed in Kelvin for each of the study areas[ref].

2.2.3 Heat vulnerability mapping

Finally, we combined vegetation trajectories, LST and insurance rates to characterize heat vulnerability across neighborhoods using principal component analysis (PCA). PCA simplifies the complexity in high-dimensional data while retaining trends and patterns. It does this by

12

transforming the data into fewer dimensions, which act as summaries of features. PCA reduces data by geometrically projecting them onto lower dimensions called principal components (PCs), with the goal of finding the best summary of the data using a limited number of PCs[ref]. Our study includes a change in tree cover to assess trends in the benefit derived from this environmental good, trend in LST to understand heat exposure and access to health insurance as an approximation of risk from its exposure. Though vulnerability assessment is not a new concept, it emerges in the climate science and policy application (Füssel & Klein, 2006) which is the first step in minimizing the impact of the future extreme climate based on socio-ecological system (Adger, 2006; Howden et al., 2007). Vulnerability provides the foundation for risk level assessment as well as building resilience (Salinger, Sivakumar, & Motha, 2005). Assessing vulnerability to heat is important for characterizing the risks posed by climate change and delivers information for recognizing measures in order to adapt to the adverse impacts of climate change. Coastal region has been marked as vulnerable due to the impacts from various activities such as continuing high density of socio economic activities, rising of temperature and changing of precipitation patterns (Moser & Davidson, 2015). In the context of climate change, assessment of vulnerability in coastal areas is found essential (McInnes et al., 2013). In multivariate statistics, Principal Components Analysis (PCA) is a mainstay of modern data analysis tool that is widely used (Blasius and Greenacre, 2014; Bro & Smilde, 2014; Hair, Black, Babin, Anderson, & Tatham, 2006; Hou, Li, & Zhang, 2015; Kline, 2014; Shlens, 2014; Yeater, Duke, & Riedell, 2015) to depict the profile of vulnerability (Kang, Xuxiang, & Jing, 2015; Guillard-Gonçalves, Cutter, Emrich, & Zêzere, 2015; Singh & Vedwan, 2015) in making decisions based on spatial maps (Okey, Alidina, & Agbayani, 2015; Schiavinato & Payne, 2015). PCA approach provides several potential advantages. When the original variables are correlated, the higher orders Principal Components (PCs) are able to capture more of the total variability in the original data than any individual original variable. PCA technique is applied for spatially

explicit aggregation of socioeconomic vulnerability (Miller, 2014), poverty (Howe, Suich, van Gardingen, Rahman, & Mace, 2013) and health vulnerability (Fisher, Ellis, Adams, Fox, & Selig, 2015; Zhu et al., 2014, Uddin, Md Nasir, et al., 2019)

3. Results

3.1 Land Cover classification

3.1.1 Results of Land Cover classification

Classification accuracy (Table. 2) measures indicate high reliability of our results comparable to numerous other land cover studies (Zeng, Hongwei, et al., 2020, Becker, Willyan Ronaldo, et al., 202, Clerici et al., 2017 , Hasan, et al., 2021). Producer's and user's accuracy and Kappa values show slight improvements comparing classifications using HR and SEN. Visual assessment comparing the two imagery shows larger amounts of speckling in the HR classification due to the higher resolution. Overall classification accuracy in 2006, 2008, 2012, 2018 and 2020 are 86.36%, 87.59%, 97.73%, 90.49% and 89.93% respectively, with Kappa indexes of 0.8793, 0.8889, 0.8862, 0.9012 and 0.9009 respectively. The comparison between classification accuracy between the different imagery suggests some differences that are negligible when at local neighborhood trends (i.e., census tract averages).

Land cover classes	2006		2008		2012		2018		2020	
	Producer's accuracy(%)	User's accuracy(%)	Producer's accuracy(%)	User's accuracy(%)	Producer's accuracy(%)	User's accuracy(%)	Producer's accuracy(%)	User's accuracy(%)	Producer's accuracy(%)	User's accuracy(%)
Water	87.54	91.21	88.23	88.34	90.31	90.24	88.36	83.24	92.89	85.01
Impervious surface	77.21	85.68	80.95	85.92	91.39	79.69	84.55	87.16	90.65	82.37
Grass / herbaceous	92.35	94.34	95.32	94.27	90.79	90.49	92.34	92.37	88.73	87.49
Tree / forest	97.89	92.69	96.70	92.02	93.66	92.39	93.77	97.46	90.69	90.15
Soil / Barren	93.08	88.75	84.45	90.88	87.30	87.33	82.85	91.42	89.81	90.53
Overall accuracy(%)	86.36		87.59		87.73		90.49		89.93	
Kappa coefficient	0.8793		0.8879		0.8862		0.9012		0.9009	

Table. 2 Classification accuracy verification values

Land cover classes	2006 - 2008		2008 - 2012		2012 - 2018		2018 - 2020		2006 - 2020	
	Area/Km^2	Area(%)	Area/Km^2	Area(%)	Area/Km^2	Area(%)	Area/Km^2	Area(%)	Area/Km^2	Area(%)
Water	-0.1988	-0.8392	-1.3724	-5.8426	1.9768	8.9379	-0.5638	-2.3400	-0.1582	-0.6678
Impervious surface	0.9190	2.8405	1.5687	4.7147	2.2382	6.4240	-0.2995	-0.8077	4.4264	13.6815
Grass / herbaceous	0.4296	1.8870	-3.0633	-13.2060	-2.273	-11.2900	0.7829	4.3836	-4.1238	-18.1134
Tree / forest	0.0623	0.3695	2.2618	13.3654	1.9153	9.9835	1.5354	7.2768	5.7748	34.2505
Soil / Barren	-1.2121	-6.3887	0.6052	3.4076	-3.8573	-21.0029	-1.455	-10.0287	-5.9192	-31.1988

Table. 3 Changes of Land cover from 2006 to 2008, 2012, 2018, 2020, and 2006 to 2020

Classification results (Fig. 3, Table. 3, Fig. 4) show substantial increases in tree cover after Hurricane Katrina over the 15-year time-span of our data, tree cover increased by over 5.8 km^2, which is a 34.3% increase for the main urban areas of NOLA. Increases can clearly be seen in parks, parkways and neighborhoods due to natural return and re-greening efforts to replace the loss of trees (Lewis, Joshua A., et al., 2017). For instance, for residential areas such as Gentilly terrace, Broadmoor and Seventh ward, gains of trees on

15

residents around neighborhoods. In City park, the reconstruction of the golf course in 2015, resulted in substantial regreening with only minimal benefits to adjacent neighborhoods. Meanwhile, impervious surfaces increased from 32. to 26.7797 km^2, a 13.6815 % decrease. Canopy regrowth and impervious expansion caused a 18.1134% decline in grass and herbaceous areas (22.76to 18.64 km^2), as these became obscured with net forest cover of increases (16.86 to 22.63 km^2). Findings suggest that some impervious surface is now shaded by the increase of tree canopy, while the other transitions include planting and management of grass, and improves in investing resources to determine the appropriate protection for levee systems (Raff, et al., 2018). The bare land area over this time decreased from 18.97 to 13.05km^2, a 31.1988% loss. This can result from the controlling of emergent vegetation and managing abandoned urban land for returning residents in repopulated flooded neighborhoods are likely causes of this loss (Lewis, Joshua A., et al., 2017).
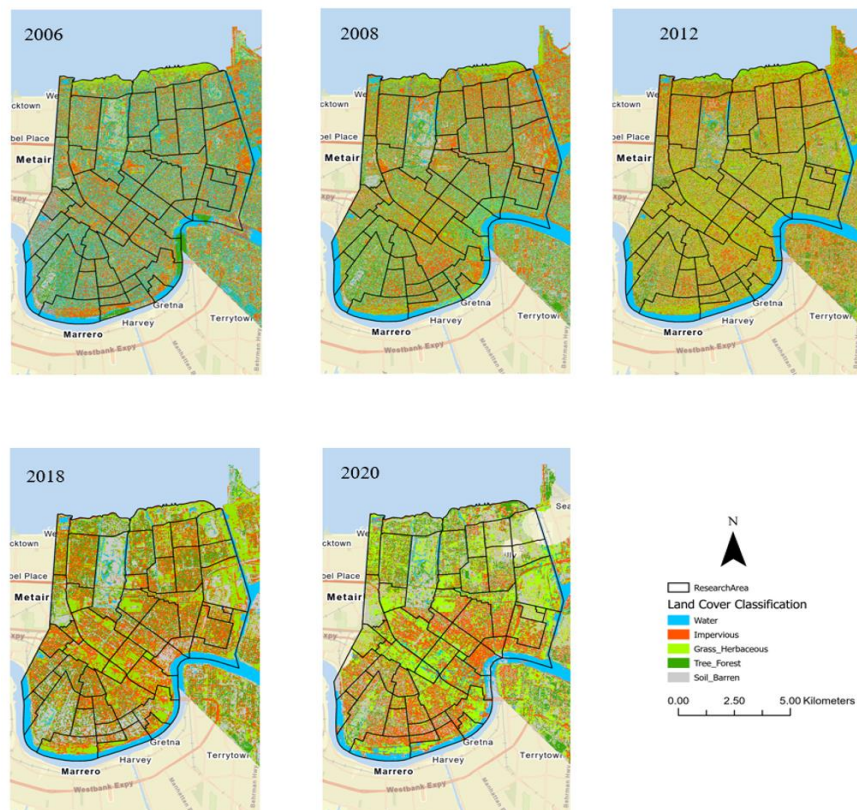

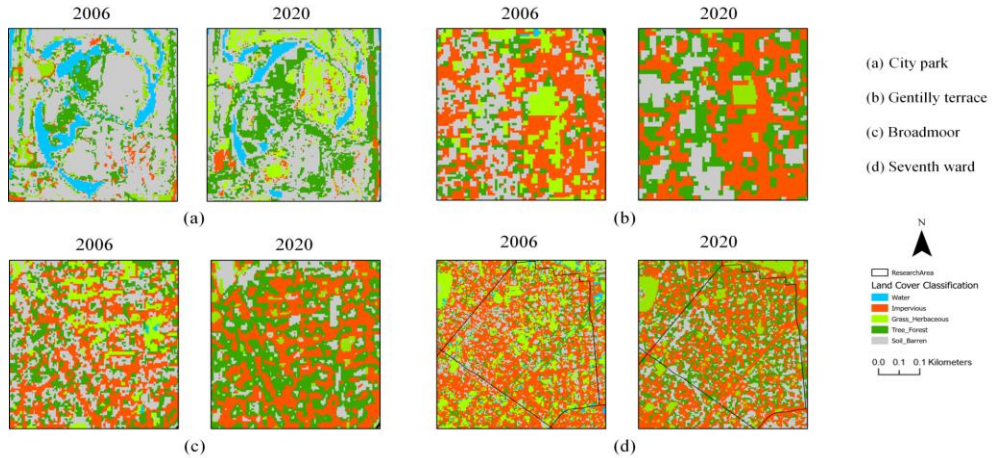Fig. 3 The Land Cover classification map in 2006, 2008, 2012, 2018 and 2020

Fig. 4 Examples of tree cover increase in parks, parkways and neighborhoods from 2006 to 2020

3.1.2 Analysis of interannual

Analysis of interannual changes (Fig. 5) suggests that tree regrowth has increased most between 2008 and 2020 after steady increases since Hurricane Katrina. Analysis of tree canopy transitions suggest that increases have come from maintaining trees on public property such as neutral grounds and in parks, and trees between the sidewalk and street. Those trees serve as natural systems and infrastructure. They can also better stave off flooding, reduce pollution, improve community health, and provide beauty and shade.
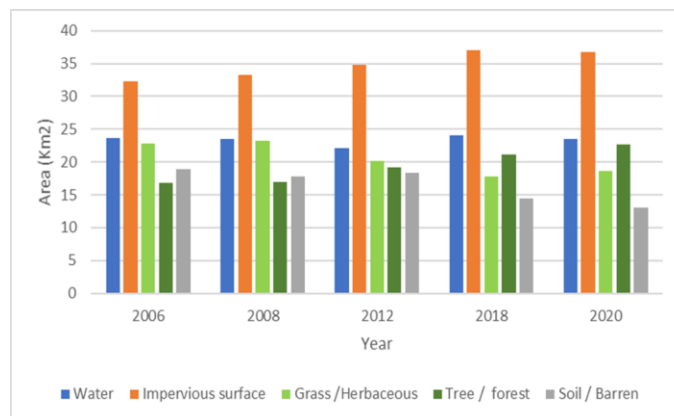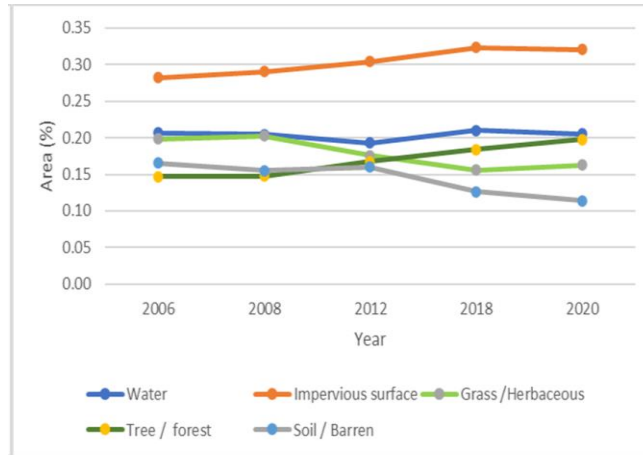
Fig. 5 Land cover change statistics from 2006 to 2020 in research area

Reconstruction and dredging can be clearly seen with river width narrower between 2012 than 2006, and increasing from 2012 to 2020. The area of impervious surface is the largest in the study area which could be the impact of reconstruction and new development urbanization according to records of the City of New Orleans. Grass and bare land changes correlate with urban expansion and limited management of natural disasters.

3.1.3 Neighborhood change

Neighborhood analysis of canopy change since the hurricane (Fig. 6) shows that increases have not been felt equally across neighborhoods with many losing tree cover over this period. Residential areas such as the Treme Lafitte, Uptown, Garden district and Central city have actually experienced loss since the Hurricane. Among tracts with increases, those located in the Lake view and Gentilly areas like St. Bernard (around 0.8 km2), and Audubon (around 1 km2) have experienced the highest percentage of tree cover increase. These residential neighborhoods were particularly hard hit by flooding when levees broke. Tract with large natural areas like City park also increased canopy as trees have rebounded after stress caused by flooding (around 1 km2 gain). Comparison of absolute and percent change neighborhood indicate that canopy in the southeast part of NOLA has lost or stagnated over the 15-year

18

period. Lack of dynamics is likely related to low possibility for increases due this area including high density residential and commercial areas marked by impervious surfaces. Tree cover was less disturbed in areas at higher surface elevations that experienced lower flooding depths, like the audubon and Lakeshore neighborhoods. Prominently, tree cover loss in the Lower garden district and the central business district exceeded that of Lakeview and Gentilly, despite having higher elevation profiles. However, the expansion of tree cover between 2006 and 2020 was greater in neighborhoods with widespread residential demolitions, land abandonment, and state management (seventh ward, St. Bernard) as opposed to neighborhoods with the lowest mean elevations (Treme laffite, central city).
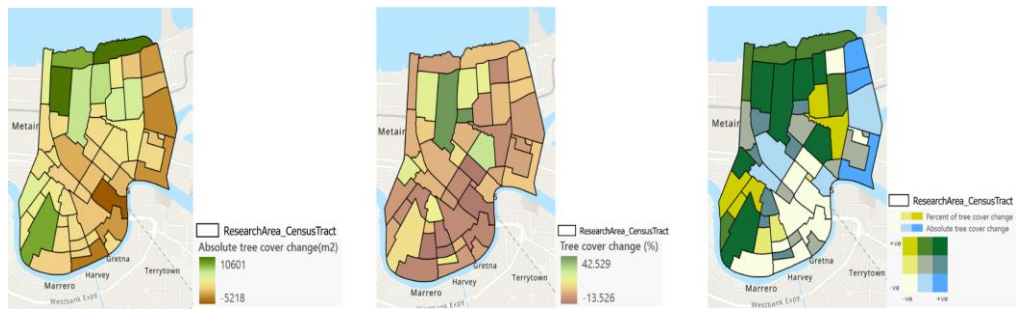

Fig. 6 Percentage of tree cover change and absolute tree cover change within census tracts in the research area from 2006 to 2020 Jenks class intervals

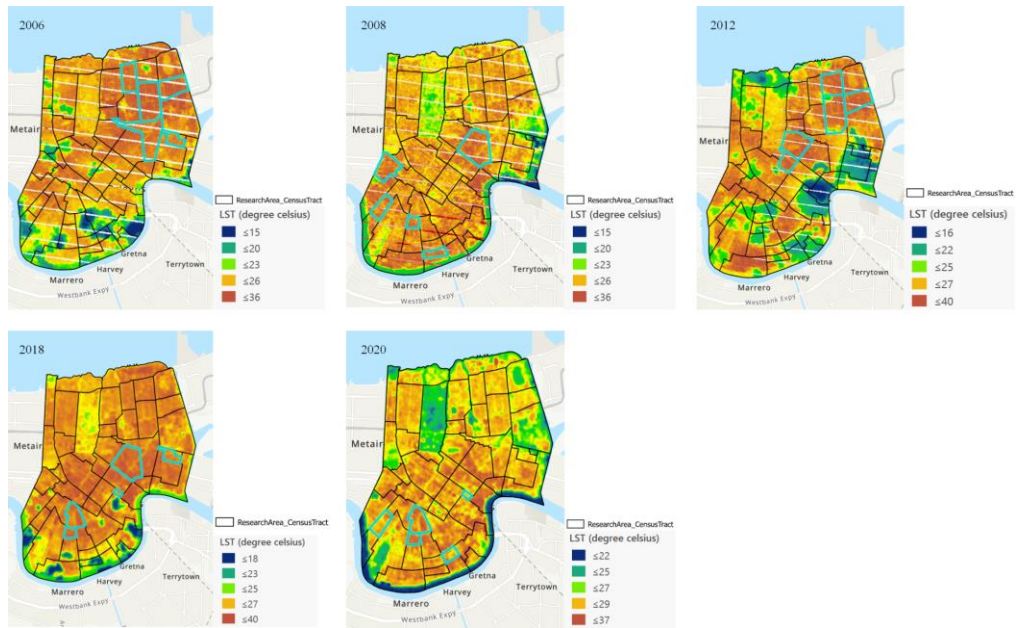3.2 Urban Heat Island analysis

Fig. 7 Land surface temperature in 2006, 2008, 2012, 2018 and 2020

Overall, average, max and min summer months LST has increased over the 16-year time period after Hurricane (Fig. 7). This has occurred even as canopy has increased. Over the period average temperature rose by 4.37 degree celsius and max and min changed by 2 and 10 degree celsius respectively. Interannual variation, peak LST in 2015 and lows in 2010, are typical for NOLA variable weather patterns marked by difference in rainfall and subsequent cooling from evapotranspiration and other extreme weather events (Hurricanes). LST also varies between neighborhoods over this period (2006 and 2020). While this is partially related to tree canopy, which is elaborated below, micro climate also plays a role in these differences (Fig. 8). For example, warm and humid southerly winds from the Gulf of Mexico can be felt in coastal neighborhoods. Landscape composition also influences these micro climate processes with highly urban areas experiencing greater wind flow compared to those with tree canopy. Among all tracts, Central city, lower garden district and Central business district have the highest percent of LST change. Those regions are mainly located around downtown and might be influenced by southerly wind and the urban heat island. Regions such as Gentilly wood, Gentilly terrace, Folmore have the lowest percentage change.

Those cities are located mainly around Gentilly and Lake view on Lake Pontchartrain which also has a regulating impact. The absolute change of LST ranges from -4 to 10 Degree celsius. Central business district and Irish channel which are located around downtown, have the biggest change. Lake terrace & oaks, Lakeshore lake vista, City park, Audubon, Fillmore, Gentilly terrace have the smallest absolute change. Those areas are located around Lake view and Gentilly. In general, the northern part of the research area has lower values for both percent change and absolute change, while the southern part has higher values. The results contrast that of tree cover change.
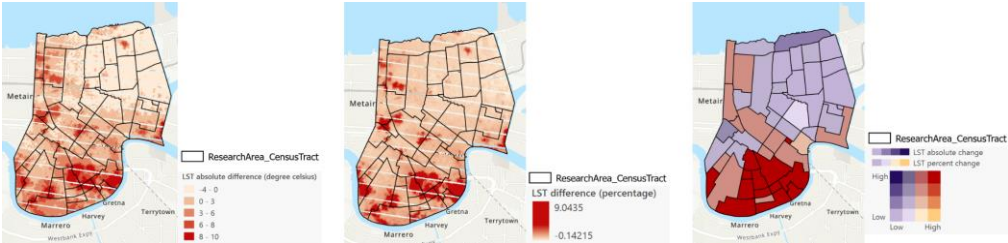

Fig. 8 Absolute and percent change of LST from 2006 to 2020

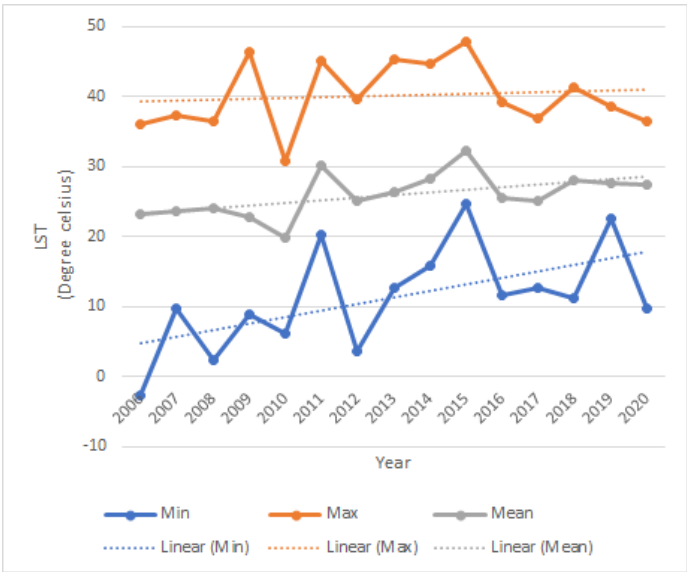3.3 Tree cover and Land Surface Temperature analysis

Fig. 9 Weekly-basis LST from 2006 to 2020 in summer months

From Fig. 9, the percent change of LST is mainly within a mild range which is -10 to 10%, and the percent change of tree cover is mainly within -10 to 50%. Analysis of the regulating impact of tree cover across neighborhoods suggests that there is no significant difference between the change of tree cover and LST (Fig. 10). This could be due to the strong southerly wind that prevails in the area, and although there is change in trees, the regulating effect of them is not obvious.
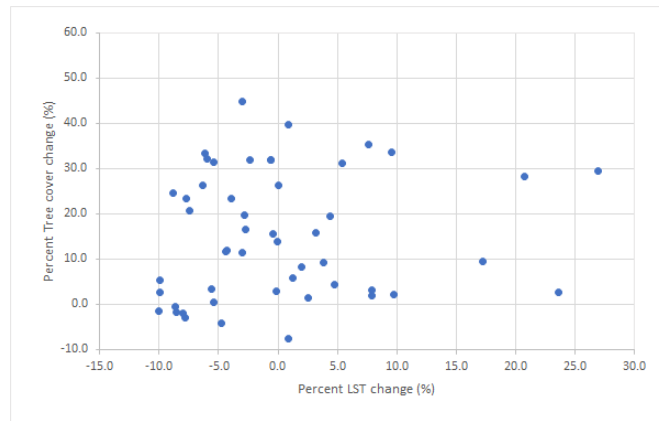

Fig. 10 Percent change of Tree cover and LST
from 2006 to 2020 by Census Tracts

3.4 Heat Vulnerability assessment

3.4.1 Health insurance coverage analysis

Our spatial analysis of heat vulnerability includes neighborhood level health insurance coverage (Fig. 11), distributions of this coverage is highly variable throughout NOLA (0 to 378). Regions such as Lake Terrace & Oaks, Mid-city, St. Anthony, Treme lafitte and Balck Pearl have higher rates of coverage, while Lakeshore-Lake vista, City park, Audubon and Desire area have lower in comparison. Those people are mainly from 19 to 64 years old. Reflecting the more limited availability of public coverage in some tracts, adults are more likely to be uninsured than children. Most uninsured people have at least one worker in the family. Families with low incomes are more likely to be

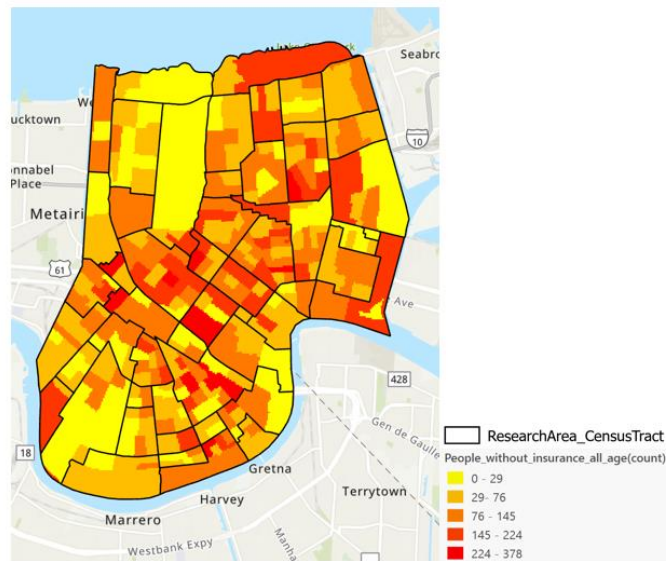uninsured. Those families at higher risk are mainly black people and located in the hurricane-prone areas.

Fig. 11 People without health insurance at all ages in 2017 in research areas

3.4.2 Principal component analysis

Our characterization of vulnerability using PCA indicated 4 distinct neighborhoods types (Table. 4). Component 1 explains 98.63% of proportion variance with eigenvalues(ev) that suggest neighborhoods with high LST (ev = 0.7008), and tree canopy (ev =0.6215) dynamics that have substantial impervious surfaces (ev = 0.3892), in areas with high rates of uninsured individuals (ev = 0.5791). PC2 has similar rates, but appears to be located in more rural areas with less impervious surface and lower change in LST. PC3 and PC4 describes neighbors with high rates of health insurance, likely in the suburbs with low rates of impervious service. The main difference is neighborhoods mapping high in PC4 experience high canopy dynamics are measured and tabulated in Table (Eigen analysis of the correlation matrix for environmental and social impact). Their coefficients are used to calculate scores. Notably, all neighborhoods will experience an increase in LST.

Together, the first two principal components represent 99.7% of the total variability representing the clearest dimensionality related to heat

vulnerability. Mapping of PCA 1 and 2 indicate the most vulnerable neighborhood given local heat trends and insurance rates. The Central business district, Irish channel, Lower garden district, Bywater and Desire area have the highest vulnerability according to the intensity of LST, tree cover, impervious surface and uninsured people. Those areas are mainly located in the central, southern and eastern parts of the research area. Tracts such as Lake view, Lake terrace & oaks, Audubon and Fillmore which are in the northern and western parts have lower vulnerability. (Fig. 12) The result implies that areas with less trees, higher LST, higher uninsured people, more impervious areas are more vulnerable and are located mainly in the southern part of the research area.

Eigenvalue	8.8018	0.0459	0.0063	0.0024
Proportion	0.9863	0.0107	0.0002	0.0001
Cumulative	0.9996	0.9999	1.0000	1.0000
Variable	PC1	PC2	PC3	PC4
Percent change of LST	0.7008	0.5825	0.8999	0.8926
Percent change of Tree cover	0.6215	0.2690	-0.5826	0.5631
Percent of People without health insurance	0.5791	0.3249	-0.1193	-0.4748
Percent of Impervious surface	0.3892	-0.6735	-0.6101	0.1321

Table. 4 Eigen analysis of the correlation matrix
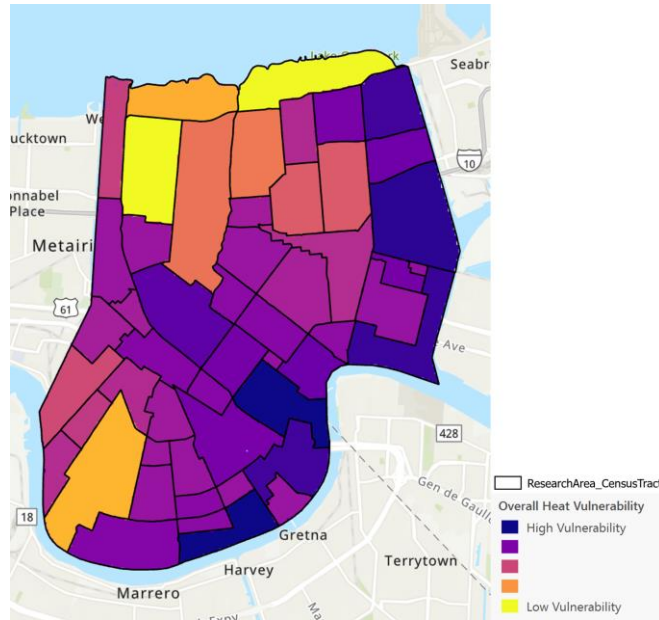
for environmental and social impact

Fig. 12 PCA Heat vulnerability in 2017 in research areas

4. Discussion and conclusion

In this study, we used high resolution orthoimage and Sentinel-2 MSI data to detect land cover change for a large portion of New Orleans, La to reconstruct canopy cover dynamics after Hurricane Katrina. We analyzed the relationship of these changes to change in LST to understand vulnerable neighborhoods. LST trends suggest increasing summer average temperature and increasing extremes between minimums and maximums. While there is likely a slight moderating impact of canopy return on these increasing temperatures, neighborhood variability is influenced by microclimatic conditions. Further analysis should explore the possible moderating impact of tree canopy increases (average Min and Max temperature). Climate change is likely to drive increasing temperature, and this will disproportionately impact residents without access to health insurances. Our methodology effectively captures current vulnerability and areas where future green intervention might moderate increasing temperature at the city-wide scale.

Change analysis typically relies on data from the same sensor or suite of sensors, which removes problems associated with change of GSD, spectral resolution, and radiometric calibration. However, because fine spatial resolution sensors cover small swaths and require large revisit times, it is often necessary to complete change mapping with multiple sensors and/or platforms (Elmes, Arthur, et al., 2017). Results of land cover showed that tree cover increased by over 5.8 km^2 from 2006 to 2020, which is a 34.3% increase for the main urban areas of NOLA. Neighborhood analysis of canopy change shows that increases have not been felt equally across neighborhoods with many losing trees covers over this period. Residential areas such as the Treme Lafitte, Uptown, Garden district and Central city have actually experienced loss since the Hurricane. Among tracts with increases, those located in the Lake view and Gentilly areas like St. Bernard and Audubon have experienced the highest percentage of tree cover increase.

To analyze the heat changes and influences in the region, LST from Landsat 7 & 8 from 2006 to 2020 were obtained. Overall, average, max and min summer months LST has increased over the 16-year time period after Hurricane Katrina. This has occurred even as canopy has increased. Over the period average temperature rose by 4.37 Degree Celsius and max and min changed by 2 and 10 Degree Celsius respectively. Among all tracts, Central city, lower garden district and Central business district have the highest percent of LST change. Those regions are mainly located around downtown and might be influenced by southerly wind and the urban heat island. Despite the re-greening in the region, the local climate still differs across neighborhoods.

The statistics results mentioned above notably shows that a formulation of heat vulnerability related with variations in tree cover, health insurance coverage and impervious surface, can enable the region to initiate its regreening projects and efforts to expand health insurance coverage at all

ages. It also found that expanding tree cover and health insurance coverage can mitigate the heat vulnerability. Our results indicate that the long-run benefits of regreening and expansion of health insurance are substantial.

Chronology of hurricanes and other extreme events have been hitting New Orleans in a long period of time. Exposure to high temperatures, which can be the result of damage of extreme events to the environment, is a serious health hazard. The human thermoregulatory system cannot offset extreme heat, resulting in a significant increase of heat related morbidity and mortality (Johnson et al., 2005, Stafoggia et al., 2006). In Louisiana, the health survey in 2017 is particularly important, as it will be the first to assess coverage after Louisiana's Medicaid expansion in 2016, which is the largest expansion of coverage for adults since the original introduction of the Medicaid program decades ago (Louisiana health insurance survey). We did a PCA analysis using tree cover, LST, impervious surface and health insurance coverage data to assess the heat vulnerability in
the region. The result implies that areas with less trees, higher LST, higher uninsured people, more impervious areas are more vulnerable and are located mainly in the southern part of the research area. It also found that expanding tree cover and health insurance coverage can mitigate the heat vulnerability which indicates that the long-run benefits of regreening and expansion of Health insurance is substantial.

For future research, ground truth data for canopy and temperature may be obtained. Additionally, community engagement, the process of working collaboratively with and through groups of people in the neighborhoods to address issues affecting the well-being of people is a powerful vehicle for bringing about environmental changes that will improve the health of the community and its members.

References

Liu, Shuxian. "Spatial and Topological Analysis of Urban Land Cover Structure in New Orleans Using Multispectral Aerial Image and Lidar Data." (2020).

Tran, Duy X., et al. "Characterizing the relationship between land use land cover change and land surface temperature." *ISPRS Journal of Photogrammetry and Remote Sensing* 124 (2017): 119-132.

Wu, Sai, et al. "Efficient B-tree based indexing for cloud data processing." *Proceedings of the VLDB Endowment* 3.1-2 (2010): 1207-1218.

Bolund, Per, and Sven Hunhammar. "Ecosystem services in urban areas." *Ecological economics* 29.2 (1999): 293-301.

Zhou, Tianyi, and Dacheng Tao. "Godec: Randomized low-rank & sparse matrix decomposition in noisy case." *Proceedings of the 28th International Conference on Machine Learning, ICML 2011.* 2011.

Pathak, Puneet, Nishi Kant Bhardwaj, and Ajay Kumar Singh. "Optimization of chemical and enzymatic deinking of photocopier waste paper." *BioResources* 6.1 (2011): 447-463.

Yang, Jun, et al. "The urban forest in Beijing and its role in air pollution reduction." *Urban forestry & urban greening* 3.2 (2005): 65-78.

Nowak, David J., Daniel E. Crane, and Jack C. Stevens. "Air pollution removal by urban trees and shrubs in the United States." *Urban forestry & urban greening* 4.3-4 (2006): 115-123.

Ng, Derrick Wing Kwan, Ernest S. Lo, and Robert Schober. "Energy-efficient resource allocation in OFDMA systems with large numbers of base station antennas." *IEEE Transactions on Wireless Communications* 11.9 (2012): 3292-3304.

Tajima, Yuhki. "The institutional basis of intercommunal order: Evidence from Indonesia's democratic transition." *American Journal of Political Science* 57.1 (2013): 104-119.

Wong, L-H., and C-K. Looi. "Vocabulary learning by mobile-assisted authentic content creation and social meaning-making: two case studies." *Journal of computer assisted learning* 26.5 (2010): 421-433.

Lewis, Joshua A., et al. "Socioecological disparities in New Orleans following Hurricane Katrina." *Ecosphere* 8.9 (2017): e01922.

Potter, Christopher. "Vegetation Cover Changes in Neighborhoods of New Orleans Following Catastrophic Flooding from Hurricane Katrina." *Applied Spatial Analysis and Policy* 14.1 (2021): 153-166.

Ortega-Farías, Samuel, et al. "Estimation of energy balance components over a drip-irrigated olive orchard using thermal and multispectral cameras placed on a helicopter-based unmanned aerial vehicle (UAV)." *Remote Sensing* 8.8 (2016): 638.

Chen, Gongbo, et al. "A machine learning method to estimate PM2. 5 concentrations across China with remote sensing, meteorological and land use information." *Science of the Total Environment* 636 (2018): 52-60.

Randall, Mark, et al. "Geographic object based image analysis of worldview-3 imagery for urban hydrologic modelling at the catchment scale." *Water* 11.6 (2019): 1133.

Gibbes, Cerian, et al. "Application of object based classification and high resolution satellite imagery for savanna ecosystem analysis." *Remote Sensing* 2.12 (2010): 2748-2772.

Civco, Daniel L., et al. "A comparison of land use and land cover change detection methods." *ASPRS-ACSM Annual Conference.* Vol. 21. 2002.

Wang, Jiong, et al. "The exposure of slums to high temperature: Morphology-based local scale thermal patterns." *Science of the total environment* 650 (2019): 1805-1817.

Lambin, Eric F., and Daniele Ehrlich. "Land-cover changes in sub-Saharan Africa (1982–1991): Application of a change index based on remotely sensed surface temperature and vegetation indices at a continental scale." *Remote sensing of environment* 61.2 (1997): 181-200.

Lu, Xinglin, et al. "In situ surface chemical modification of thin-film composite forward osmosis membranes for enhanced organic fouling resistance." *Environmental science & technology* 47.21 (2013): 12219-12228.

Hansen, James, et al. "Global surface temperature change." *Reviews of Geophysics* 48.4 (2010).

Kogan, Felix, Tatiana Adamenko, and Wei Guo. "Global and regional drought dynamics in the climate warming era." *Remote Sensing Letters* 4.4 (2013): 364-372.

Voogt, James A., and Tim R. Oke. "Thermal remote sensing of urban climates." *Remote sensing of environment* 86.3 (2003): 370-384.

Wan, Qing, et al. "Fabrication and ethanol sensing characteristics of ZnO nanowire gas sensors." *Applied Physics Letters* 84.18 (2004): 3654-3656.

Leng, Pei, et al. "Bare surface soil moisture retrieval from the synergistic use of optical and thermal infrared data." *International Journal of Remote Sensing* 35.3 (2014): 988-1003.

Zhao, Zhengli, Dheeru Dua, and Sameer Singh. "Generating natural adversarial examples." *arXiv preprint arXiv:1710.11342* (2017).

Nichol, Janet E., et al. "Urban heat island diagnosis using ASTER satellite images and 'in situ'air temperature." *Atmospheric Research* 94.2 (2009): 276-284.

Breiman, Leo. "Random forests." *Machine learning* 45.1 (2001): 5-32.

Zafari, Azar, Raul Zurita-Milla, and Emma Izquierdo-Verdiguier. "Evaluating the performance of a random forest kernel for land cover classification." *Remote sensing* 11.5 (2019): 575.

Chan, Jonathan Cheung-Wai, et al. "An evaluation of ensemble classifiers for mapping Natura 2000 heathland in Belgium using spaceborne angular hyperspectral (CHRIS/Proba) imagery." *International Journal of Applied Earth Observation and Geoinformation* 18 (2012): 13-22.

Belgiu, Mariana, and Lucian Drăguţ. "Random forest in remote sensing: A review of applications and future directions." *ISPRS journal of photogrammetry and remote sensing* 114 (2016): 24-31.

Berhane, Tedros M., et al. "Decision-tree, rule-based, and random forest classification of high-resolution multispectral imagery for wetland mapping and inventory." *Remote sensing* 10.4 (2018): 580.

Pilant, Andrew, et al. "US EPA EnviroAtlas Meter-Scale Urban Land Cover (MULC): 1-m Pixel Land Cover Class Definitions and Guidance." *Remote sensing* 12.12 (2020): 1909.

Congalton, Russell G. "A review of assessing the accuracy of classifications of remotely sensed data." *Remote sensing of environment* 37.1 (1991): 35-46.

Keshtkar, Hamidreza, Winfried Voigt, and Esmaeil Alizadeh. "Land-cover classification and analysis of change using machine-learning classifiers and multi-temporal remote sensing imagery." *Arabian Journal of Geosciences* 10.6 (2017): 1-15.

Uddin, Md Nasir, et al. "Mapping of climate vulnerability of the coastal region of Bangladesh using principal component analysis." *Applied geography* 102 (2019): 47-57.

Zeng, Hongwei, et al. "A synthesizing land-cover classification method based on Google earth engine: a case study in nzhelele and levhuvu catchments, South Africa." *Chinese Geographical Science* 30.3 (2020): 397-409.

Becker, Willyan Ronaldo, et al. "Statistical features for land use and land cover classification in Google Earth Engine." *Remote Sensing Applications: Society and Environment* 21 (2021): 100459.

Clerici, Nicola, Cesar Augusto Valbuena Calderón, and Juan Manuel Posada. "Fusion of Sentinel-1A and Sentinel-2A data for land cover mapping: a case study in the lower Magdalena region, Colombia." *Journal of Maps* 13.2 (2017): 718-726.

Hasan, Sumaya Falih, Muntadher Aidi Shareef, and Nihad Davut Hassan. "Speckle filtering impact on land use/land cover classification area using the combination of Sentinel-1A and Sentinel-2B (a case study of Kirkuk city, Iraq)." *Arabian Journal of Geosciences* 14.4 (2021): 1-12.

Raff, Edward, Jared Sylvester, and Steven Mills. "Fair forests: Regularized tree induction to minimize model bias." *Proceedings of the 2018 AAAI/ACM Conference on AI, Ethics, and Society*. 2018.
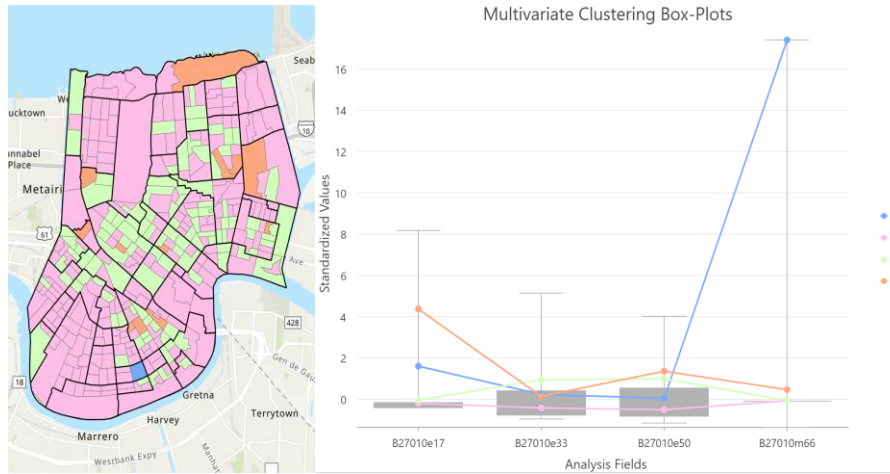
Indexes

Fig. (Distribution of people without health insurance at different age groups. B27010e17: people under 19 years old, B27010e33: people between 19 and 34 years old, B27010e50: people between 34 and 64 years old, B27010m66: people older than 65)

Image	High resolution orthoimage						Sentinel-2 MSI			
Land cover classes	2006		2008		2012		2018		2020	
	Area/Km²	Area(%)	Area/Km²	Area(%)	Area/Km²	Area(%)	Area/Km²	Area(%)	Area/Km²	Area(%)
Water	23.6883	0.2066	23.4895	0.2049	22.1171	0.1929	24.0939	0.2102	23.5301	0.2052
Impervious surface	32.3533	0.2822	33.2723	0.2902	34.841	0.3039	37.0792	0.3234	36.7797	0.3208
Grass / herbaceous	22.7666	0.1986	23.1962	0.2023	20.1329	0.1756	17.8599	0.1558	18.6428	0.1626
Tree / forest	16.8605	0.1471	16.9228	0.1476	19.1846	0.1673	21.0999	0.1841	22.6353	0.1974
Soil / Barren	18.9725	0.1655	17.7604	0.1549	18.3656	0.1602	14.5083	0.1266	13.0533	0.1139
Total	114.6412	1.0000	114.6412	1.0000	114.6412	1.0000	114.6412	1.0000	114.6412	1.0000

Fig. Land cover classification in 2006, 2008, 2012, 2018 and 2020